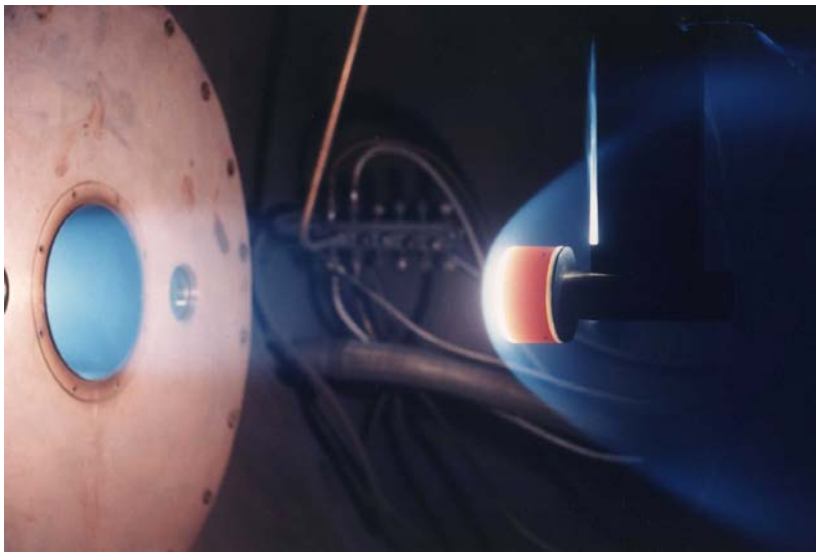

Figure 1: High temperature non-equilibrium flow phenomena around a capsule

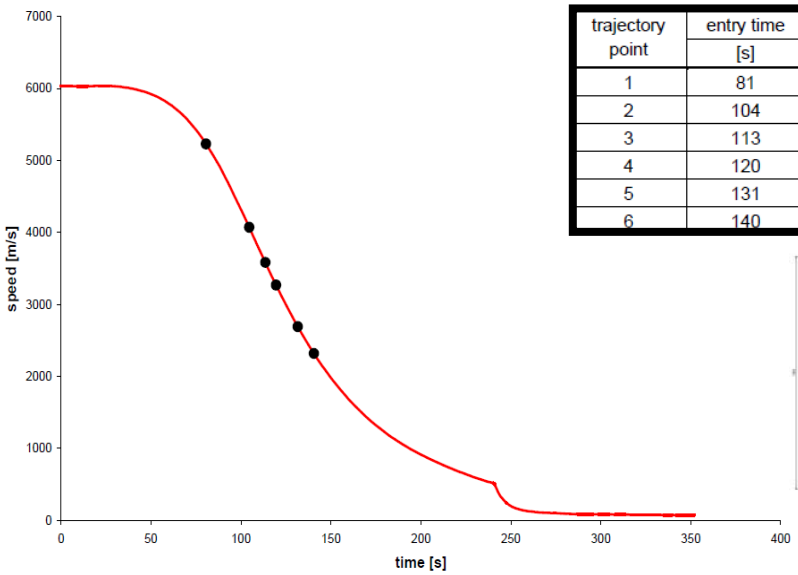

trajectory point	entry time [s]	velocity [m/s]	enthalpy [MJ/kg]	Pitot pressure [hPa]
1	81	5228	13.8	55
2	104	4072	8.5	82
3	113	3581	6.6	82
4	120	3266	5.5	79
5	131	2691	3.8	70
6	140	2317	2.9	62

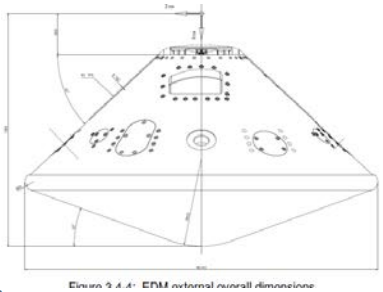

Fig. 2: Selected SACOMAR trajectory points [2].

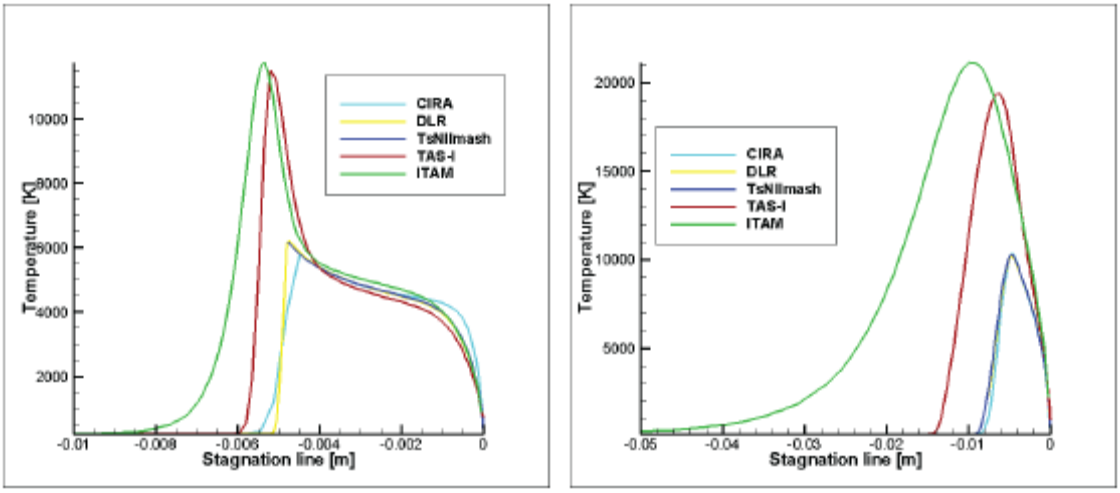

Fig. 3: Computed stagnation line temperature for TP1 (left) and TP2 (right) [3].

Table 1: Temperature model of different codes [3]

code	Temperature set
CIRA	T, Tv
DLR	T
TsNIImash	T, Tv
ITAM	Ttrasl, Trot, Tv
TAS-I	T, Tv(CO_2), Tv(N_2), Tv(O_2), Tv(NO), Tv(CO)

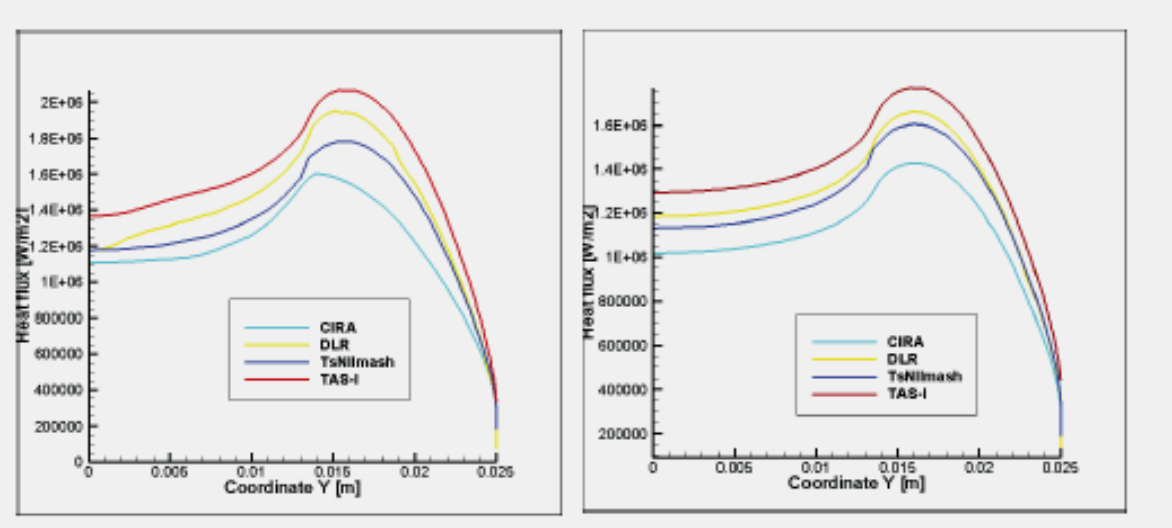

Fig. 4: Heat flux rates to the same model computed with different codes for TP 1 (left) and TP 2 (right) [3].

Table 2: Computed heat fluxes with different codes [3]

Case	CIRA (Fluent)	DLR (TAU)	TsNIImash	ITAM (SMILE)	TAS-I
std_tp1_fc	1100	1175	974		1096
std_tp2_fc	980	1185	924		1039
std_tp1_nc	700	688	515	802	709
std_tp2_nc	610	723	508	1101	710
lrg_tp1_fc	650	651	677		709
lrg_tp2_fc	590	715	614		602
lrg_tp1_nc	350	415	332		349
lrg_tp2_nc	260	307	262	482	275

Table 3: EXOMARS test matrix [4]

Test facility	Test condition	enthalpy [MJ/kg]	Pitot pressure [hPa]	model diameter [mm]
U-13	FC-1	13.8	80,40,20,10	50
	FC-2	9.0	80,40,20,10	50
IPG-4	FC-1	13.8	80,40	50
	FC-2	9.0	80,40	50
L2K	FC-1	13.8	80,20,10	50,100
	FC-2	9.0	80,20	50,100
HEG	FC-1	13.8	700	100
	FC-2	9.0	80	100
IT-2	FC-4	2.0	tbc	100
	FC-3	5.0	tbc	100

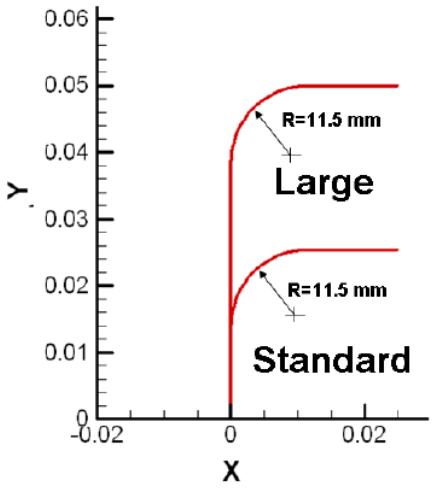

Fig. 5: Test model geometries [24]

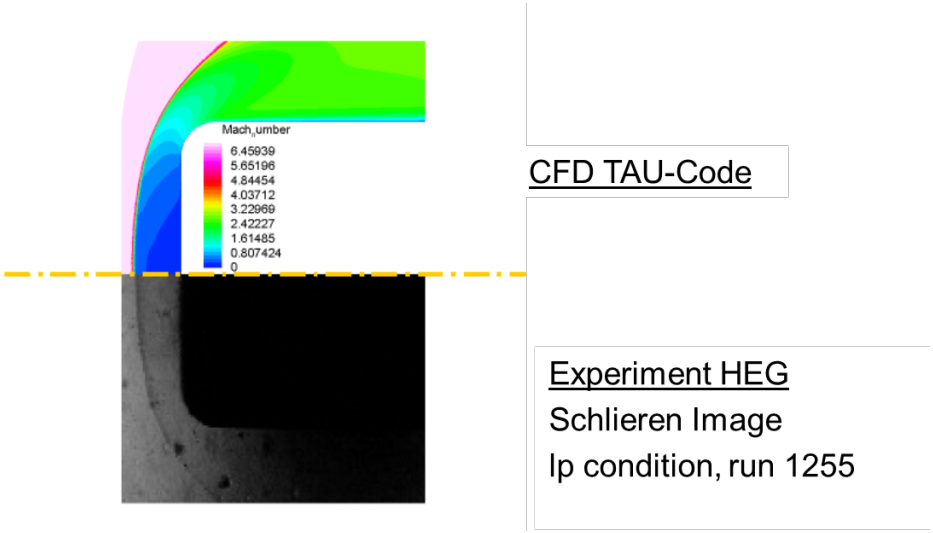

Fig. 6: Hybrid CFD Mesh around SACOMAR wind tunnel test probe (and MatchingTAU-Code Result Compared to Experimental Schlieren Image, Solution for HEG Test Condition Mach 6.86, after One Adaptation Cycle) [21][8].

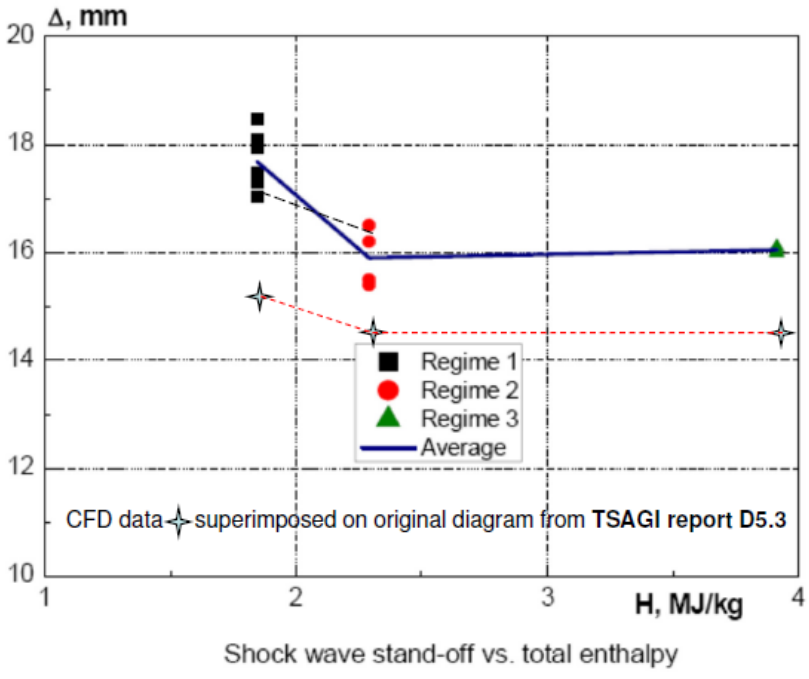

Fig. 7: Shock stand-off distances for the IT-2 regimes 1,2 and 3 [9][21].

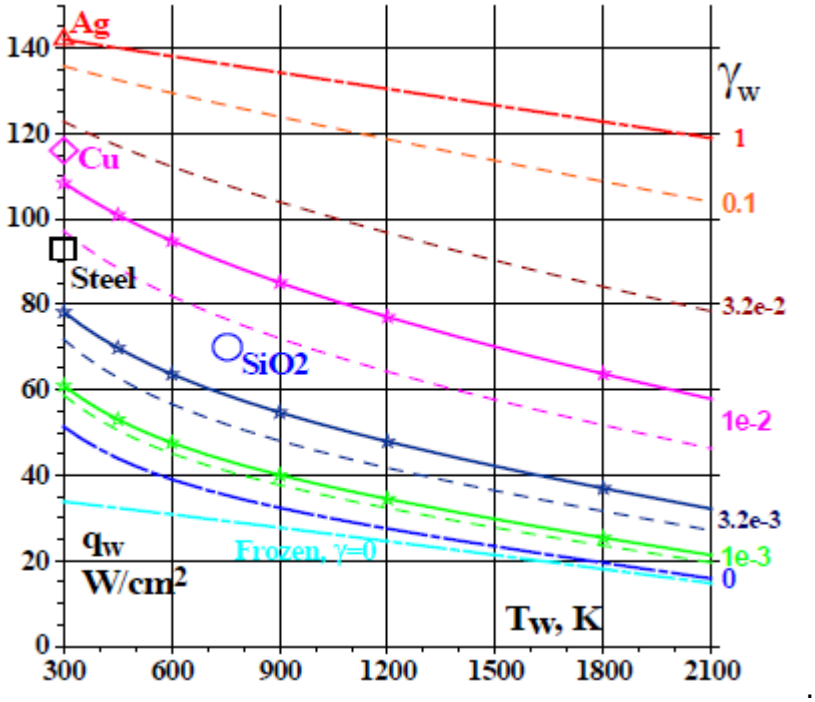

Fig. 8: Measured and computed heat flux rates for different surfaces in the Martian high enthalpy flow of the IPG-4 facility [10][22].

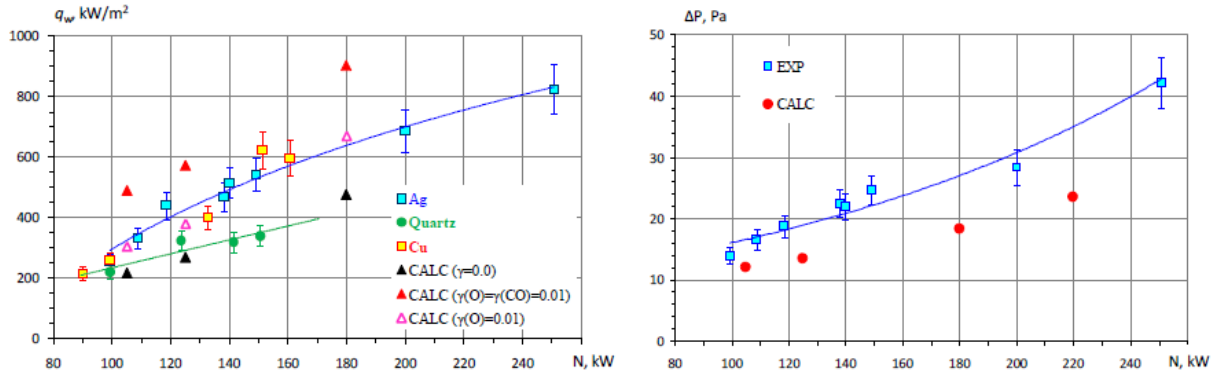

Fig. 9: Experimental and numerical heat fluxes (left) and Pitot pressures (right) at 80 mbar condition in the U-13 facility of TsNIImash [11][23].

Table 4: Comparison of heat flux measurements [12].

Test condition	Model diameter [mm]	Pitot pressure [hPa]	Heat flux rate [kW/m^2]		
			HFM	Calorimeter	
				Slug	Water-cooled
FC-1	100	20	891	640	
	50	20	1091	740	830
	50	80	-	1380	1680
FC-2	100	20	518	355	
	50	20	694	440	570
	50	80	-	630	1000

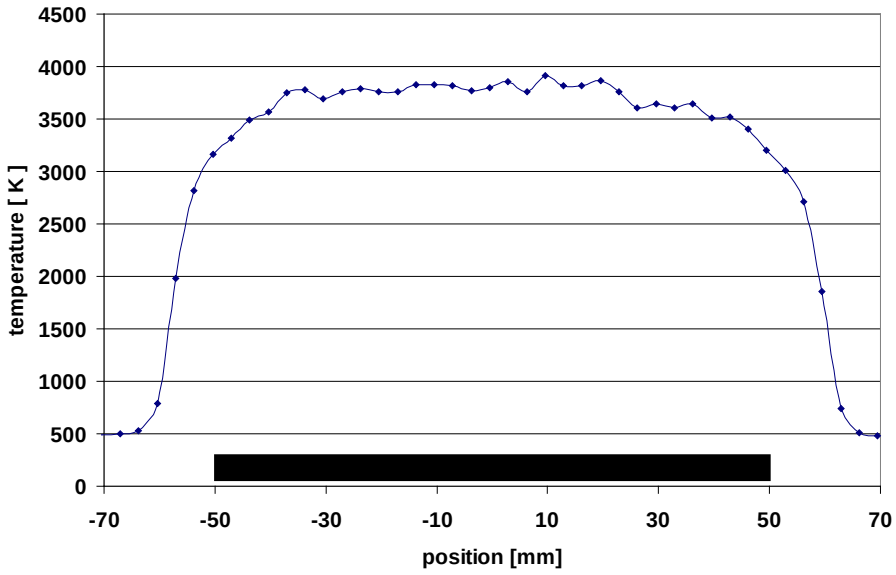

Fig. 10: Temperature profile 3 mm in front of the 100 mm model at test condition FC-1 [12].

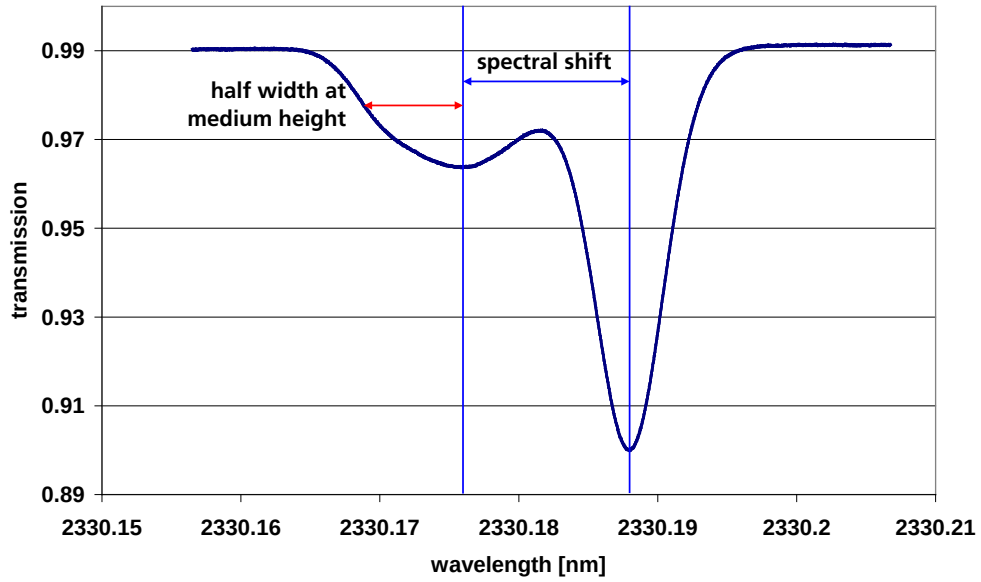

Fig. 11: Results from DLAS measurement at flow condition FC-1 [12].

Table 5: Test matrix for code-to-code validation [3]

Case	Model diameter [mm]	Mach	P∞ [Pa]	T∞ [K]	Wall
std_tp1_fc	50	17.32	22.46	222.92	fully catalytic
std_tp2_fc		30.17	0.95	155.20	
std_tp1_nc		17.32	22.46	222.92	non catalytic
std_tp2_nc		30.17	0.95	155.20	
lrg_tp1_fc	100	17.32	22.46	222.92	fully catalytic
lrg_tp2_fc		30.17	0.95	155.20	
lrg_tp1_nc		17.32	22.46	222.92	non catalytic
lrg_tp2_nc		30.17	0.95	155.20	

Table 11 - test matrix for code to code validation

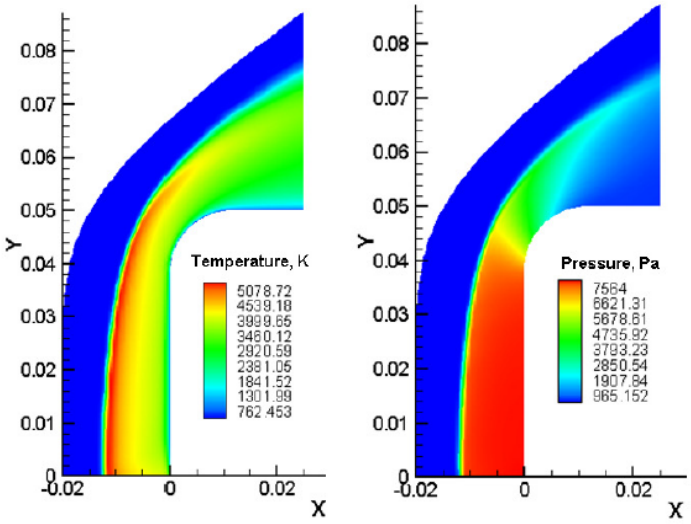

Fig. 12: Pressure and temperature contours around the larger probe at TP 1 [17].

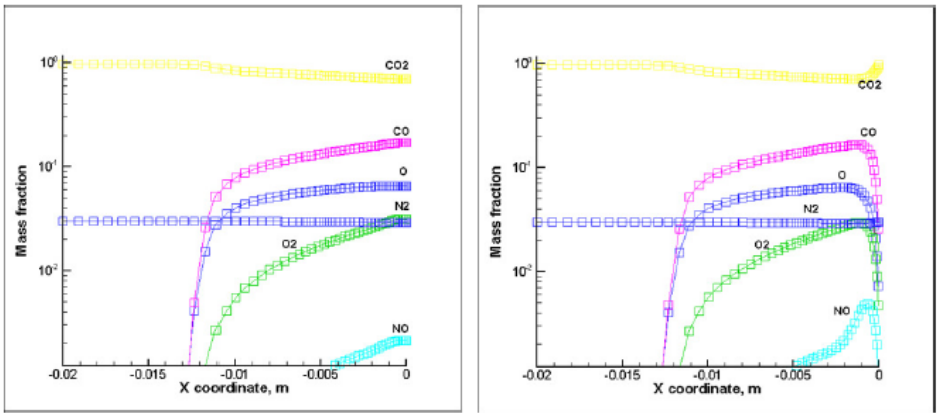

Fig. 13: Species concentrations in the shock layer of the larger probe at TP 1, non-catalytic (left) and equilibrium (right)[17].

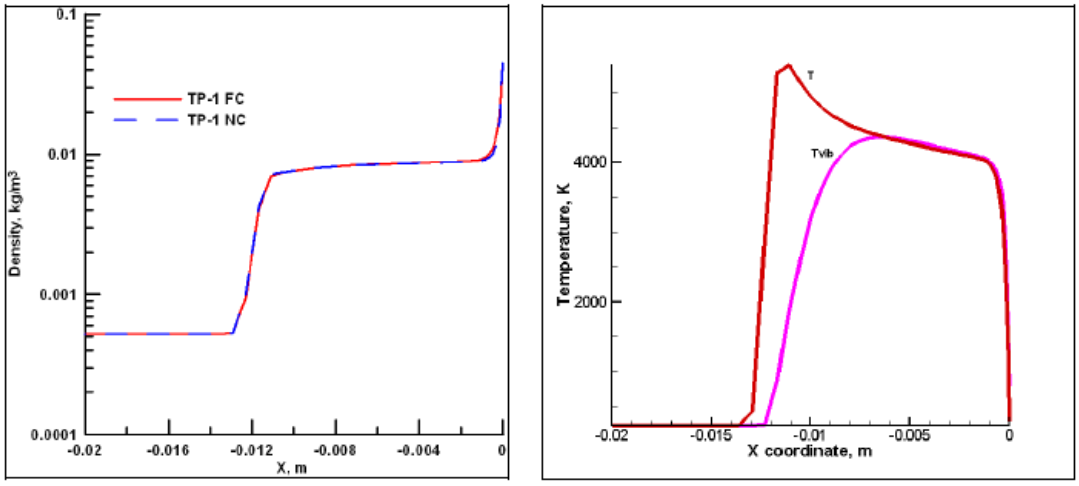

Fig. 14: Density (left) and temperature (right) profiles along the stagnation line of the larger probe at TP 1 [17].

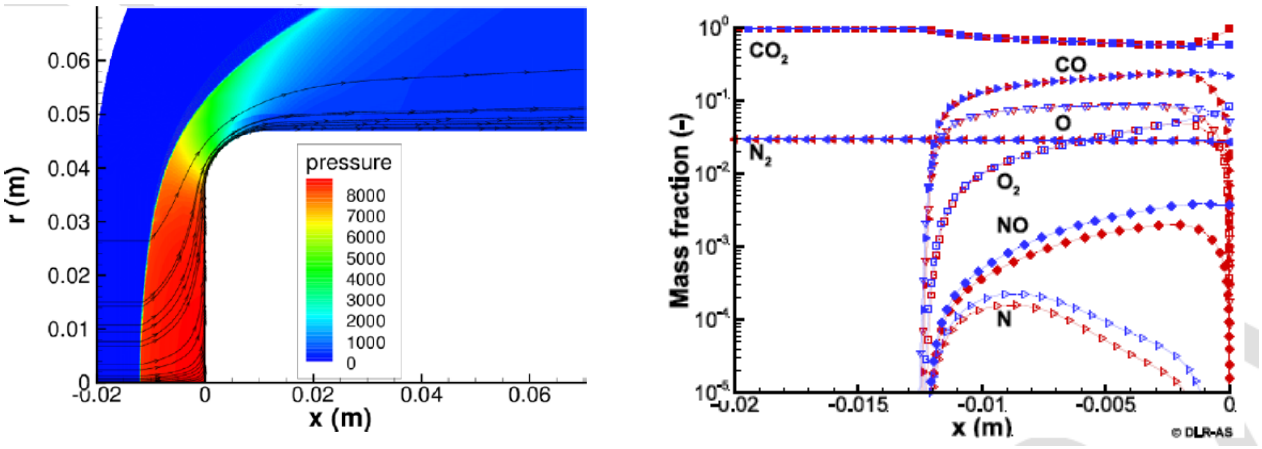

Fig. 15: Pressure contours and streamlines (left) and mass concentration (right) for the larger probe at TP 1 [18].

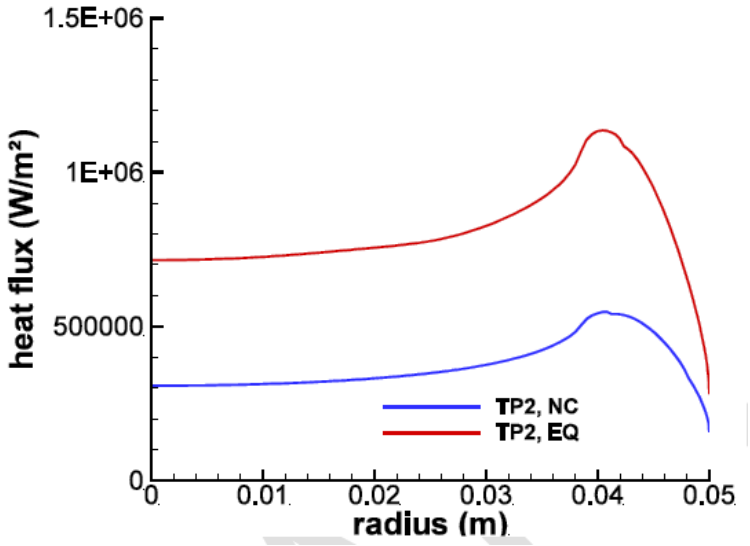

Fig. 16: Computed heat flux distribution over the surface of the larger probe at TP 2 [18].

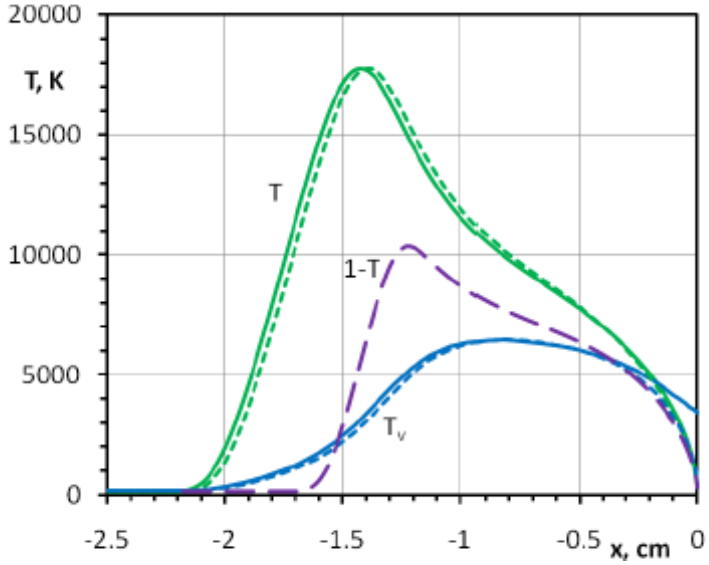

Fig. 17: Temperature evolution along the stagnation line of a non-catalytic surface, larger model at TP 2 [19].

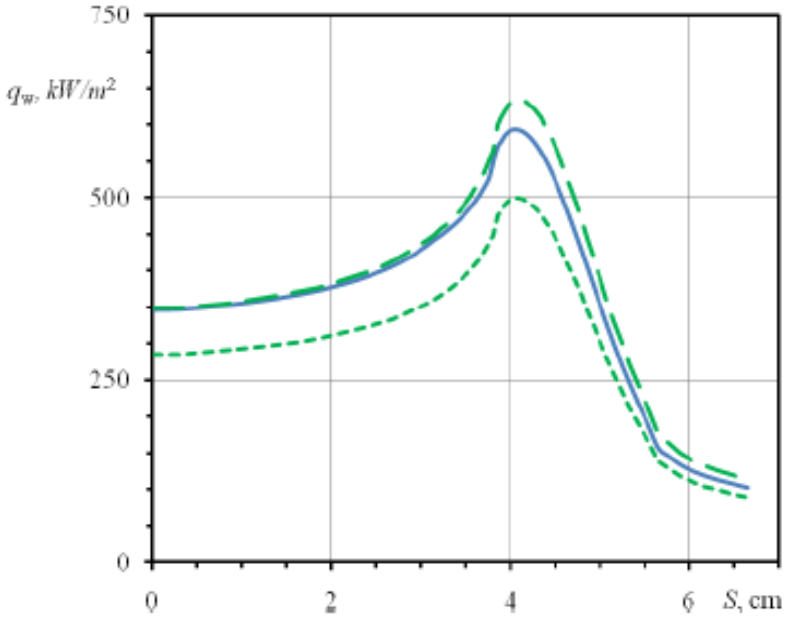

Fig. 18: Heat flux distribution over the non-catalytic surface, larger model at TP 2 [19].

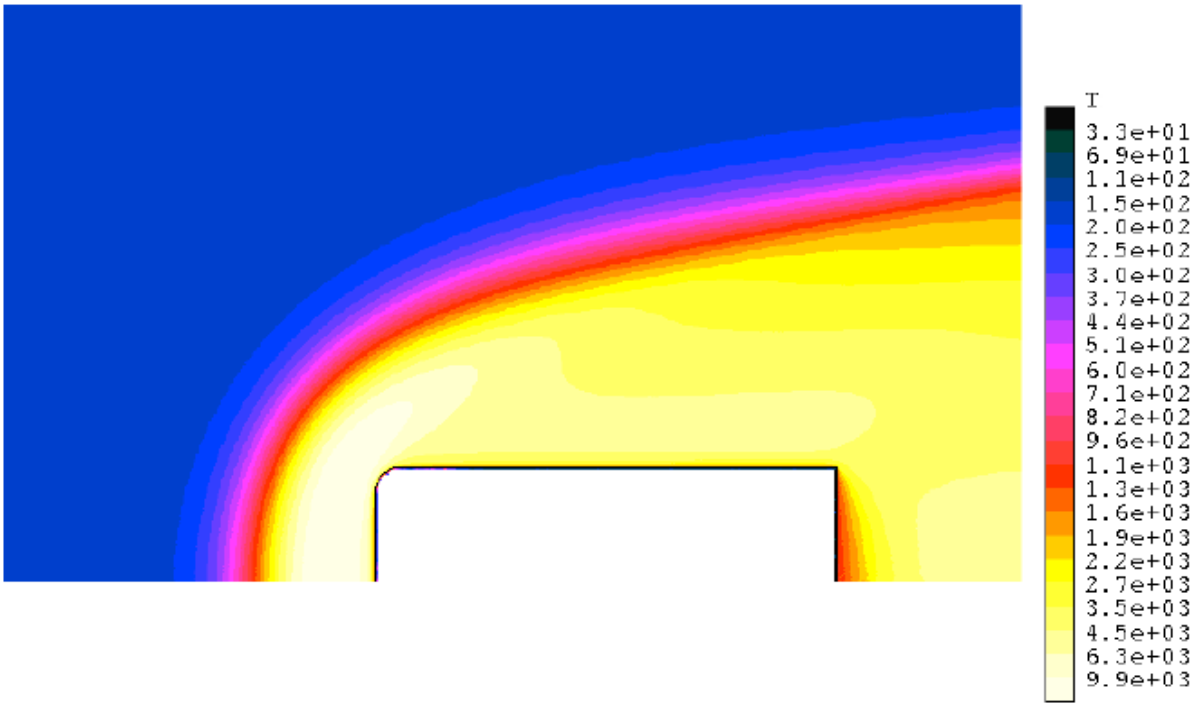

Fig. 19: Translational temperature distribution (DSMC computation by the SMILE code) around the larger model at TP 2 [20].

Figure 8. Translational temperature flowfield. Point 2. 100 mm probe.

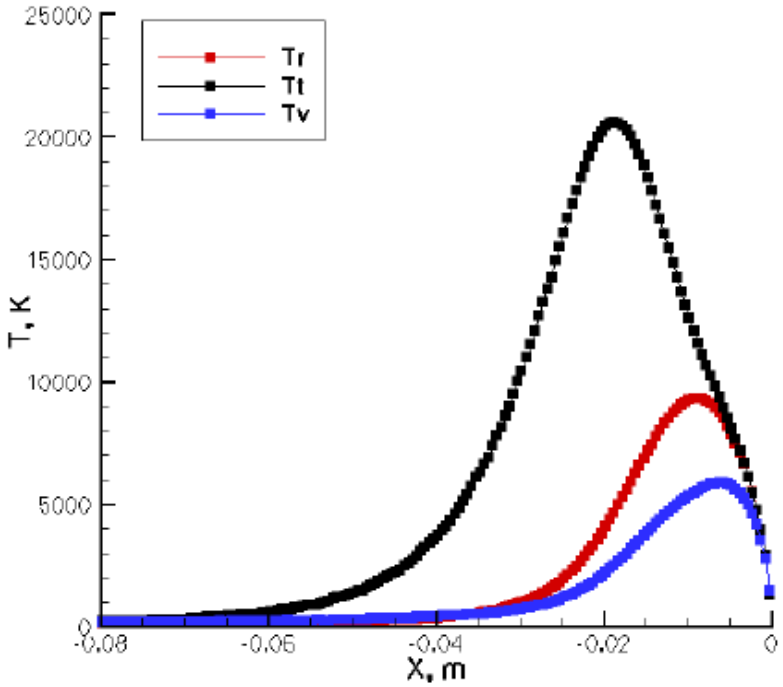

Fig. 20: Evolution of translational, rotational and vibrational temperatures along the stagnation line of a non-catalytic surface, larger model at TP 2 [20].

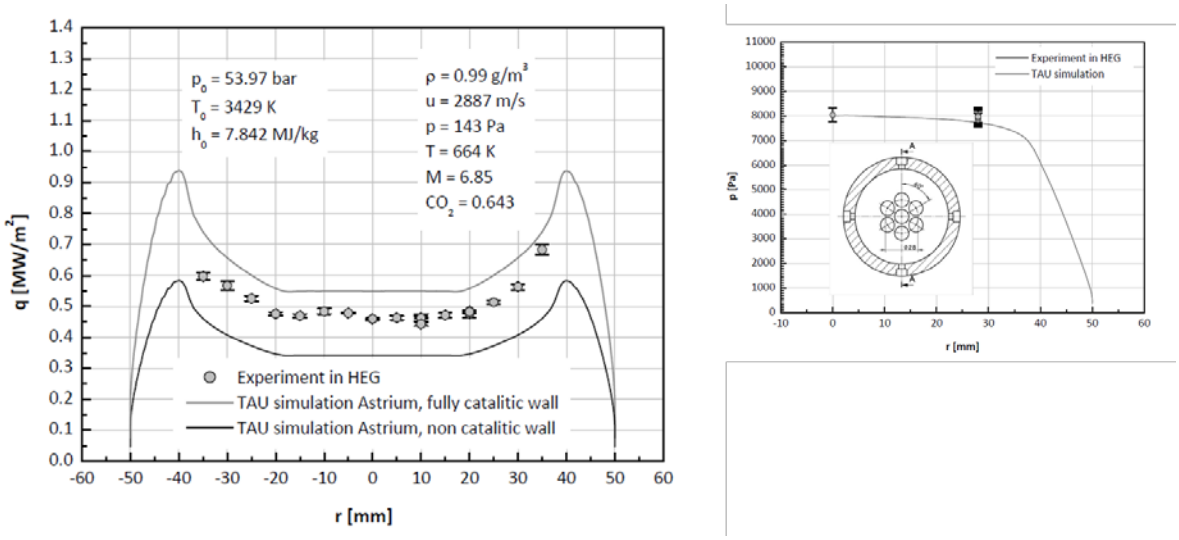

Fig. 21: Comparison HEG Condition lp , Non Catalytic and Fully Catalytic Calculation vs. Test Results [8][21].

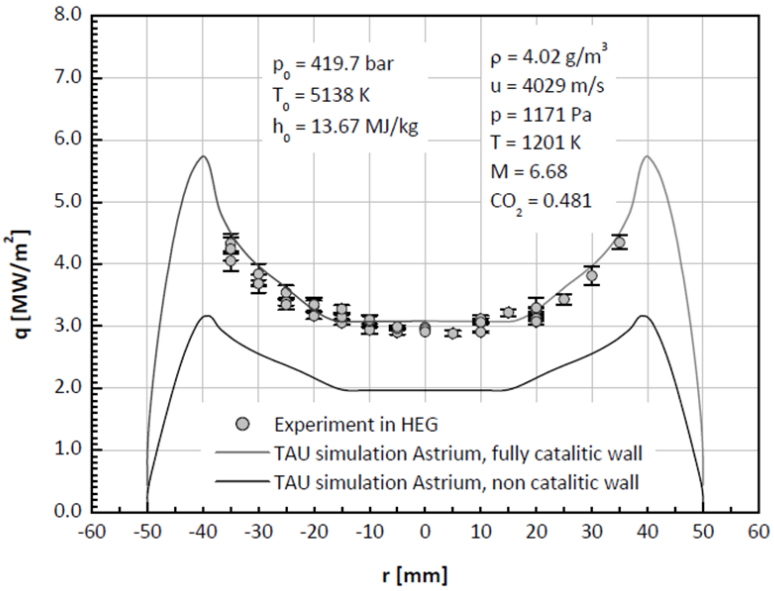

Fig. 22: Comparison HEG Condition hp, Non Catalytic and Fully Catalytic Calculation vs. Test Results [8][21].

Table 6: CO surface recombination coefficients determined using novel catalysis model [22]

P hPa	N_{ap} kW	Zm mm	testing material	T_w K	q_w W/cm^2	γ_{wO} specified by literature data	γ_{wCO} determined by novel model	$\gamma_w = \gamma_{wO} = \gamma_{wCO}$ determined previously by standard model
80	40.4	40	quartz	755	70	2e–3	6.0e-3	7.84e-3
			steel	300	93	2.6e–3	6.1e-3	8.48e-3
80	34.0	40	quartz	600	45	2e–3	3e-3	4.97e-3
			steel	300	66	2.6e–3	n/a	1.07e-2
40	35.0	72	quartz	606	46	2e–3	5e-3	5.71e-3
			steel	300	72	2.6e–3	9e-3	1.13e-2
40	35.0	122	quartz	500	30	2e–3	2e-3	3.42e-3
			steel	300	45	2.6e–3	7e-3	8.77e-3

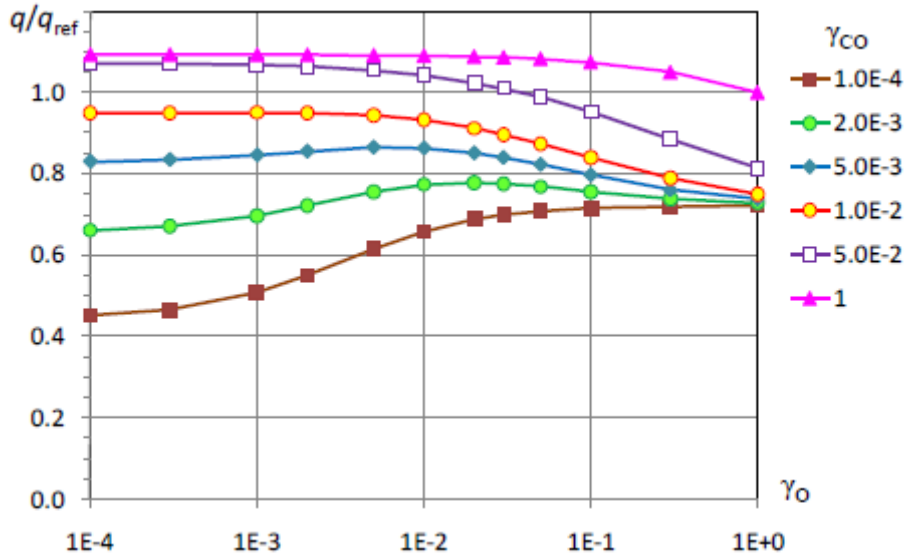

Fig. 23: Relative stagnation point heat flux rate for different recombination probabilities [23].

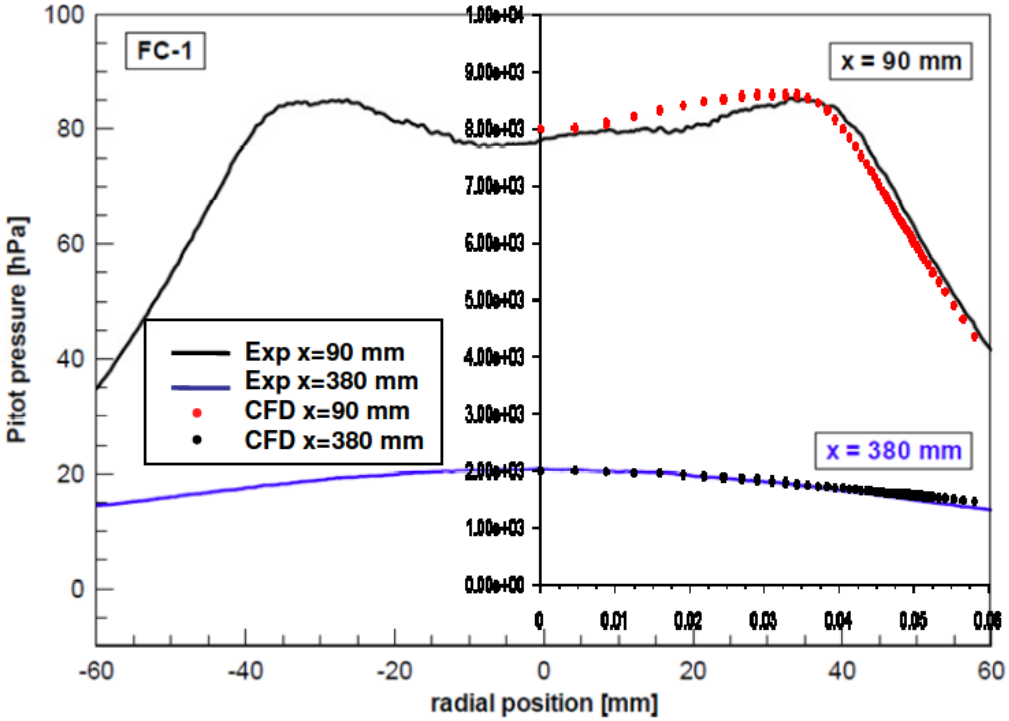

Fig. 24: Measured and computed Pitot pressures for FC-I conditions in L2K [21] [24].

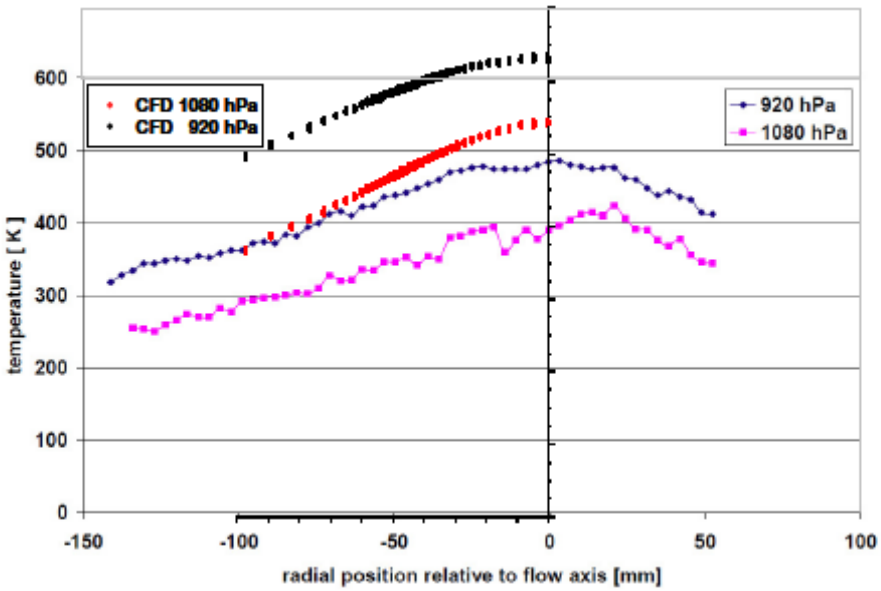

Fig. 25: Measured and computed free stream temperature profiles for both FC-I and FC-II flow conditions in L2K [12][24].

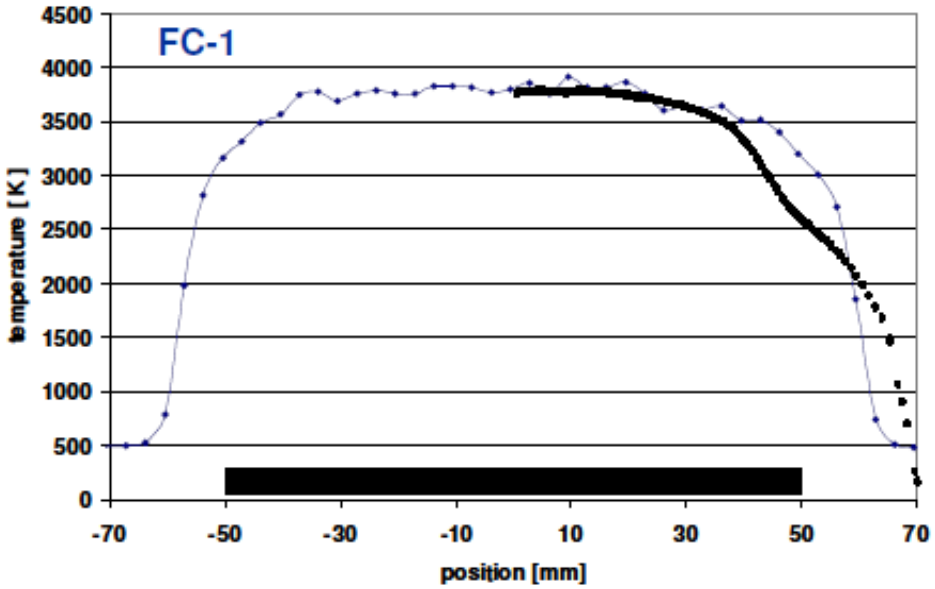

Fig. 26: Measured and computed temperature profiles in the shock layer 6 mm from the surface of the model with 100 mm diameter at 380 mm from the nozzle exit and FC-1 [12][24].

Table 7: Measured and computed heat fluxes in L2K [12][24]

Test condition	Model diameter	Pressure [Pa]				Heat flux rate [kW/m^2]				
	[mm]	Pitot pressure	CFD Pitot	S.P. pressure	CFD p02	HFM sensor	Slug (stainless steel)	Water-cooled (copper)	CFD FC	CFD NC
FC-1	100	21.6	20	-	20.3	891	640	-	820	260
	50	21.6	20	21.9	19.4	1091	740	830	1100	360
	50	77.5	80	80.1	80.9	-	1380	1680	1800	580
FC-2	100	18.5	18	-	16.2	518	355	-	500	190
	50	18.5	18	19.3	15.5	694	440	570	660	260
	50	67.6	72	69.8	69.6	-	630	1000	1200	500

References

[1] Gülhan, A., et al; SACOMAR Interim Progress Report, SACOMAR Deliverable D1.1, issue 1.0 16.12.2011.

[2] Mareschi, V.; Requirements on Modelling and Simulation, SACOMAR deliverable D 4.1, issue 1.1, 30.10.2011.

[3] Mareschi, V.; Synthesis of Results, SACOMAR deliverable D 4.2, issue 1.0, 31.07.2012.

[4] B. Esser., A. Gülhan; Test plan for Experiments, SACOMAR deliverable D 5.1, 30.6.2011.

[5] P. Nöding; Review of CO_2 Physico-Chemical Modelling and Recommendation for Improvement, SACOMAR deliverable D 6.1, Issue 1.1, 30.11.2011.

[6] Steven Sepka Yih-Kanq Chen and Jochen Marschall and Richard A. Copeland, 'Experimental Investigation of Surface Reactions in Carbon Monoxide and Oxygen Mixtures', Journal of Thermophysics and Heat, Vol. 14, No. 1, January–March 2000.

[7] Jochen Marschalll and Richard A. Copeland, Helen H. Hwang and Michael J. Wright, 'Surface catalysis experiments on metal surfaces in Oxygen and Carbon Monoxide Mixture', AIAA paper 2006-181.

[8] J. Martinez Schramm: Results of Experimental Study in the High Enthalpy Shock Tunnel Göttingen (HEG), SACOMAR Deliverable D 5.2, Issue 1.0, 21.02.2012.

[9] V.Ya. Borovoy, A.S. Skuratov, I.V. Struminskaya, E.G. Zaitsev; TsAGI Deliverable 5.3, Results of experimental study in TsAGI IT-2 Hot Shot wind tunnel, 27.02.2012.

[10] A. Koleshnikov, A. Gordeev, S. Vasilevski; Results of the experimental study in the IPG-4 facility, SACOMAR Deliverable D5.4, Issue 2.1, 30.09.2011.

[11] R. V. Kovalev, V. I. Vlasov; N. F. Rudin, G. N. Zaloginn; Results of experimental study in the TsNIImash Plasmatron Facility U-13, SACOMAR Deliverable D5.5, Issue 1.0, 30.09.2011.

[12] B. Esser, U. Koch, A. Gülhan.; Results of the experimental study in the L2K Facility, SACOMAR Deliverable D5.6, Issue 1.1, 30.06.2012.

[13] P. Nöding; Review of Physico-Chemical CO_2 Modelling and Recommendation for Improvements, SACOMAR Deliverable D6.1, Issue 1.1, 30.11.2011.

[14] R. V. Kovalev, V. I. Vlasov; G. N. Zaloginn; Modelling of CO_2+N_2 gas mixture, SACOMAR Deliverable D6.2, Issue 1.0, 30.01.2012.

[15] M. Fertig; Report and library on gas phase chemistry, SACOMAR Deliverable D6.3, Issue 1.0, 10.02.2012.

[16] A. Koleshnikov, S. Vasilevski, A. Gordeev, A. Levitin; Reprot and library on surface chemistry, SACOMAR Deliverable D6.4, Issue 1.0, 26.01.2012.

[17] Mario De Stefano Fumo; CIRA Code Modelling Validation, SACOMAR Deliverable D7.1, Issue 1.0, 14.07.2012.

[18] M. Fertig; Improvement of TAU code with respect to the modeling and numerical scheme for CO_2+ N_2 flows, SACOMAR Deliverable D7.3, Issue 1.0, 31.07.2012.

[19] R. V. Kovalev, A. G. Gorschkov, V. I. Vlasov; Improvement of the TsNIImash code with respect to the modeling and numerical scheme for CO_2+ N_2 flows, SACOMAR Deliverable D7.5, Issue 1.0, 30.03.2012.

[20] Ye. A. Bonder, M. S. Ivanov; Improvement of the TsNIImash code with respect to the modeling and numerical scheme for CO_2+ N_2 flows, SACOMAR Deliverable D7.7, Issue 1.0, 23.06.2012.

[21] P. Nöding; Numerical Simulation of HEG and IT-2 Experiments in CO_2 Flow, SACOMAR Deliverable 7.9, 15th August 2012.

[22] A. Koleshnikov, A. Gordeev, S. Vasilevski; Numerical simulation of IPG-4 experiments in CO_2+ N_2 flow, SACOMAR Deliverable D7.11, Issue 1.0, 20.03.2012.

[23] R. V. Kovalev, A. B. Gorshkov, V. I. Vlasov; Numerical simulation of experiments in the TsNIImash Plasmatron facility, SACOMAR Deliverable D7.13, Issue 1.0, 30.05.2012.

[24] Mario De Stefano Fumo; Simulation of L2K Tests, SACOMAR Deliverable D7.15, Issue 1.0, 14.07.2012.